This is a preprint, the final version is subject to change, of the American Mineralogist (MSA)
Cite as Authors (Year) Title. American Mineralogist, in press.
(DOI will not work until issue is live.) DOI: http://dx.doi.org/10.2138/am-2017-6101

First revision

Nitrides and carbonitrides from the lowermost mantle and their importance in the search for Earth's 'lost' nitrogen

Felix Kaminsky[1,*] , Richard Wirth[2]

[1]KM Diamond Exploration Ltd., West Vancouver, BC V7S3J1, Canada

[2] Helmholtz Centre Potsdam, GFZ German Research Center for Geosciences, Potsdam, Germany

Abstract

The first finds of iron nitrides and carbonitride as inclusions in lower-mantle diamond from Rio Soriso, Brazil are herein reported. These grains were identified and studied with the use of transmission electron microscopy (TEM), electron diffraction analysis (EDX) and electron energy-loss spectra (EELS). Among nitrides, trigonal Fe_3N and orthorhombic Fe_2N are present. Carbonitride is trigonal $Fe_9(N_{0.8}C_{0.2})_4$. These mineral phases associate with iron carbide, Fe_7C_3, silicon carbide, SiC, Cr-Mn-Fe and Mn-Fe oxides; the latter may be termed Mn-rich xieite. Our identified finds demonstrate a wide field of natural compositions from pure carbide to pure nitride, with multiple stoichiometries from $M_5(C,N)_3$ to $M_{23}(C,N)_6$ and M/(C,N) from 1.65 to 3.98. We conclude that the studied iron nitrides and carbonitrides were formed in the lowermost, lower mantle as the result of the infiltration of liquid metal, containing light elements, from the outer core into the D" layer, with the formation of the association: native Fe^0 + iron nitrides, carbides and transitional compounds + silicon carbide. They indicated that major reservoirs of nitrogen should be expected in the core and in the lowermost mantle, providing some solution to the problem of nitrogen balance in the Earth.

* E-mail: felixvkaminsky@aol.com

Key words: nitride, carbide, nitrogen, lower mantle

Introduction

Earlier, we reported upon finds of a series of iron carbides with admixtures of up to 7.3-9.1 at.% N (N/(N+C) = 0.19-0.27), included in lower-mantle diamonds, in association with native iron and graphite. It was established that the iron carbides formed within the Earth's core at a pressure interval of 50-130 GPa; these grains having crystallised from an iron-carbon melt, rich in nitrogen (Kaminsky and Wirth 2011). Subsequently, nitrocarbides and carbonitrides, $Fe_2(N,C)$, $Fe_3(N,C)$, $Fe_7(N,C)_3$ and $Fe_9(N,C)_4$, with 12.8-18.42 at.% N and N/(N+C) = 0.37-0.60 were identified in a lower-mantle microxenolith (Kaminsky et al. 2015). In our recent studies, we have identified as inclusions in diamond other carbonitrides and pure nitrides, which we report herein.

Nitrogen, the seventh most abundant element in the Solar System, remains one of the most enigmatic in studies of Earth's geochemistry. There is a so-called 'missing nitrogen' problem in the Earth's inner parts because, according to existing estimates, nitrogen is at one order of magnitude less than other volatile elements, with the value of bulk Earth/carbonaceous chondrite ratio equal to 0.11 % (Marty 2012). The calculated atomic ratio for N/Si in the bulk Earth is several orders of magnitude lower than that for the remaining terrestrial planets/or bodies within the asteroid forming zone (Bergin et al. 2015). As a result, nitrogen is considered as a trace element in the major silicate reservoirs (Busigny and Bebout 2013), even as "a useless element in mantle geochemistry" (Cartigny and Marty 2013) owing to extensive nitrogen outgassing during the Earth's early history (Goldblatt et al. 2009; Bergin et al. 2015; Hirschmann 2016) or in response to a giant impact(s) (Tucker and Mukhopadhyay 2014). On the other hand, Li et al. (2013) concluded that the mantle may still contain an amount of nitrogen one to two orders of magnitude larger than the present atmospheric reservoir. Nitrogen is suggested to have siderophile behavior in the core's metal alloy and extremely high solubility, with partitioning of nitrogen $K^{\text{Metal/Silicate}}$ around 10,000 (Miyazaki et al. 2004). Such high value implies a nitrogen mass, in the core, hundreds of

51 times greater than that in the atmosphere; an estimate for the total proportion of nitrogen in the core by
52 Miyazaki et al. (2004) is ~ 1×10^{24} g. This suggestion is supported by high concentrations of nitrogen in
53 iron meteorites (Sugiura 1998) and provides a basis to consider the Earth's core as a major reservoir to
54 nitrogen (Marty 2012; Roskosz et al. 2013), containing perhaps 97 % of its total planetary inventory
55 (McDonough 2014). The most recent calculations conclude that the fraction of nitrogen within the Earth's
56 core may be between 10 % and 90 %, depending upon the oxygen fugacity values in force during metal-
57 silicate equilibration, and whether the core is a significant, but not dominant reservoir of terrestrial
58 nitrogen (Dalou et al. 2016). The exact quantities of nitrogen in the core and the mantle remain unclear.
59 Here we report the first finds of iron nitrides, Fe_2N and Fe_3N, and carbonitride, $Fe_9(N,C)_4$, as
60 inclusions in lower-mantle diamond from Rio Soriso, Brazil. We suggest that iron nitrides and
61 carbonitrides are mineral phases, characteristic to the core/mantle boundary. These phases associate with
62 iron carbide, Fe_7C_3, and silicon carbide, SiC. We conclude that: (1) the presence of these minerals at the
63 core/mantle boundary is the result of the infiltration of liquid metal, containing light elements, from the
64 outer core into the D" layer, with the formation of the association: native Fe^0 + iron nitrides, carbides and
65 transitional compounds + silicon carbide; and (2) major reservoirs for Earth's nitrogen should be expected
66 in the core and in the lowermost mantle.
67
68 **Sample and Methods**
69
70 ***The crystal of diamond*** #8-103 selected for the present study is from the Juina area in Mato Grosso State,
71 Brazil. The crystal is a dodecahedroid typical of the stones from this area. It is the same sample, in which
72 earlier nyerereite, nahcolite and calcite were identified in association with periclase, wüstite and other
73 minerals (Kaminsky et al. 2009a, 2015; Wirth et al. 2009). Its dimensions are 5.2 × 4.9 × 3.8 mm.
74 Optical microscopy reveals numerous inclusions of differing size and colour within this stone. The
75 nitrogen concentration of diamond #8/103, detected with Fourier Transform Infrared Spectroscopy
76 (FTIR), is 44 ppm and consists only of B centres; *i.e.,* this is a Type-IaB diamond (Kaminsky et al.

2009b). Such low concentration and high nitrogen-aggregation ratios are characteristic of 'deep' diamond (Hutchison et al. 1999, Kaminsky et al. 2009b). Another interesting feature of this stone, like for most of the 'deep' diamond crystals of the Juina area, is a high concentration of the hydrogen impurity centres identified at 3,107 and 1,405 cm^{-1} in the IR spectrum (Wirth et al. 2009). Commonly, this centre is either absent or weakly expressed. In contrast to the majority of diamond deposits worldwide, almost all of the diamond crystals from the Juina pipes (80–89%) have noticeable (up to 4.2 cm–1) levels of the hydrogen C–H centre (Kaminsky et al. 2009b). The diamond shows high dislocation density with curved dislocation lines, homogeneously distributed throughout the crystal.

Diamond #8-103 was crushed in order to gain access to the inclusions inside the stone. Individual fragments of the diamond were selected for focused ion beam (FIB) sample preparation. Only those inclusions in the diamond situated close to the surface of fragments were selected to be suitable for FIB sample preparation and subsequent transmission electron microscopy (TEM), combined with electron diffraction analysis (EDX) and electron energy-loss spectral analysis (EELS). These analyses were performed in Helmholtz Centre Potsdam, GFZ German Research Center for Geosciences.

Electron-transparent foils were milled by FIB techniques, applying a single-beam device (FEI FIB 200 TEM) operated at GFZ Potsdam, Germany (Ga-ion beam, 30 keV acceleration voltage). The foil thicknesses varied from 100 to 150 nm. Four different foils have been cut with FIB methods from the diamond (##2327, 2934, 4588 and 4592). Details about the FIB sample preparation from diamond can be found elsewhere (Wirth 2004, 2009).

TEM was performed employing a TECNAI F20 X-Twin transmission electron microscope operated at 200 keV with a Schottky field emitter as electron source. The TEM was equipped with a Gatan imaging filter (GIF Tridiem™), a Fishione high-angle annular dark-field detector (HAADF) and an EDAX X-Ray analyser with ultrathin detector window. TEM bright-field and dark-field images, as well as high-resolution lattice fringe images were routinely acquired as energy-filtered images applying a 20 eV window to the zero-loss peak.

Electron diffraction analyses (EDX) were always performed in the scanning transmission mode (STEM), scanning the electron beam within a preselected area. Acquisition times were on the order of 120 seconds to achieve reasonable counting statistics. The concentrations of elements were quantified with the use of the TIA software package, using the k_{AB} factors provided by the software. There are no reliable k_{AB} factors available in the database for nitrogen and carbon. Therefore, quantitative analysis of N and C in iron carbides and nitrocarbides was not possible. An additional problem with quantification of carbides and nitrides from EDX spectra is the fact the fluorescence yield for N and C is very low and the few X-ray photons emitted from these elements are strongly absorbed by the matrix. Consequently, the N and the C intensities in the EDX spectra are very low.

Electron energy-loss spectra (EELS) were recorded in diffraction mode using a camera length of 700 mm according to a collection angle ß (half angle) 2 mrad. Acquisition time was 10 seconds. Data evaluation occurred using the Gatan Digital Micrograph software package. For quantification of the spectra the Hartree-Slater model was applied.

Phase identification was based upon electron diffraction analysis. Diffraction data were collected as electron diffraction patterns recorded on image plates or were calculated from high-resolution lattice fringe images applying the fast Fourier Transform algorithm (FFT). The observed *d*-spacings and the angles between adjacent planes were compared with calculated *d*-spacings and angles between adjacent lattice planes. The indexing of the diffraction pattern was accepted to be correct only if the angles between adjacent planes match the calculated angles within a deviation of < 1°.

Results

Iron nitrides

Two types of iron nitride grains were distinguished among inclusions (Table 1; Fig. 1). ***The first type*** comprise tabular or equidimensional single-phase grains, 1-2.5 μm in size (Fig. 1a). Some of such

inclusions are intergrown with smaller (300-400 nm) grains of oxides. ***The second type*** is represented by 8-10 μm elongated inclusions, consisting of an aggregate of nitride and/or replacing it polycrystalline graphite (Fig. 1b). Nitride forms irregular, 0.5-1.5-μm grains along the periphery of the aggregate and smaller (0.1-0.3 μm), irregularly-shaped, relics within the graphite matrix, demonstrating a typical structure of resorption of the initial nitride grain by graphite. In dark- and bright-field images the relic iron nitride grains show the same crystallographic orientation, confirming that they belong to a former, single large crystal. In one of the foils (#2327) both types of iron nitride grains are present.

The identification of inclusions was based on electron diffraction data (Supplementary Table 1). Type 1 inclusions were identified as Fe_3N, with a trigonal *P*312 structure (Niewa et al. 2009; type 2 (resorbed) inclusions were identified as Fe_2N, with an orthorhombic *Pbcn* structure (Rechenbach and Jacobs 1996). Diffraction patterns of the third inclusion (foil #2327; Supplementary Fig. 1) show indices, which may be based on both trigonal, Fe_3N and orthorhombic, Fe_2N structures. While both crystal systems allow for a consistent indexing of the pattern, a comparison of the measured *d*-spacings with those calculated for the two possible nitride phases favours the orthorhombic phase; Fe_2N, better matches the calculated data (Table 1). The diffuse and strongly smeared-out diffraction spots in the electron diffraction pattern (Supplementary Fig. 1) suggest a mosaic structure of the grain with numerous subgrains that are slightly misoriented with respect to each other. The individual subgrains may belong to a single phase or to two different iron nitride phases.

EDX spectra from the nitride inclusions demonstrate the presence of Fe, N, Cr, Ni, Mn and Si (Fig. 2). The cation compositions of the nitrides, calculated from the obtained EDX spectra, are dominated by iron (90.8-97.13 at.%), with admixtures of Cr (0.68-1.8 at.%), Ni (0.35-0.93 at.%) and Mn (0-1.22 at.%). Of particular interest is the presence of 5.1-7.6 at.% of Si in Fe_2N (Supplementary Table 2).

Iron carbonitride

In addition to pure nitrides, in one of the inclusions (#4588) a carbonitride, $Fe_9(N_{0.8}C_{0.2})_4$, grain, 6 × 7 μm in size was identified (Fig. 3). It has straight, sharp interfaces with the host diamond, except for the area in the upper part of the image, where the inclusion is corroded, - possibly by a fluid in a pore, which opened during the course of the focussed ion beam (FIB) sample preparation. The identification of this phase as $Fe_9(N_{0.8}C_{0.2})_4$ was available from the electron diffraction data (Leineweber et al. 2001) (Supplementary Table 3). The EDX and EEL spectra of carbonitride indicate the presence of three major elements Fe, N and C and an admixture of Si, like in some of the iron nitrides (Supplementary Fig. 2).

Iron carbide

Two straight lamellae of 100-500 nm thickness cut the hosting iron carbonitride grain (Figs. 3 and 4a). Judging from the EDX and EEL spectra (Fig. 4b,c,d), they do not contain nitrogen; only iron and carbon are present, with the ratio Fe/C = 2.46, close to the ideal ratio for Fe_7C_3 (2.33). This composition is confirmed by the electron diffraction data (Bouchard 1967), according to which the lamellae are of an orthorhombic iron carbide, Fe_7C_3 (Supplementary Table 4).

Silicon carbide

The iron carbide lamellae are heterogeneous in both structure and composition. The main body of the lamellae (grey in Figs 3 and 4a) comprise only Fe and C. High-resolution images, however, demonstrate that within the iron carbide some brighter areas occur, which form plate-like, cubic and irregular areas, 50-200 nm in size, and occupying ~5-10 % of the entire lamellae volume (Figs 3 and 4a). EDX spectra measured from these areas demonstrate that they are composed of Si and C (Fig. 4d). Because of the nanometre-size of these crystallites, many of which are less than the foil thickness, a Fe K_α peak occurs in their EDX spectra. Fe is contributed from the host Fe-carbide. The Si-C areas have specific *d*-spacings in electron diffraction patterns (0.2332 nm; 0.2172 nm; 0.1731 nm and 0.149 nm; Supplementary Table 4),

179 which cannot be attributed to Fe_7C_3, but match the hexagonal 6H polytype of silicon carbide according to
180 Capitani et al. (2007). A drift-corrected elemental map, using the Si*K*α and C*K*α X-ray intensities,
181 demonstrates strong enrichment in Si and C of a cubic inclusion in the lamellae (Fig. 5) and confirms its
182 identification as SiC.
183
184 **Oxides**
185
186 Both iron nitride and carbonitride are intergrown with smaller (200-800 nm) oxide grains. One of the
187 grains intergrown with carbonitride, $Fe_9(N_{0.8}C_{0.2})_4$ (Fig. 3), according to electron-diffraction data, has a
188 cubic spinel-like structure. There are several micro-pores between this grain and the carbonitride, which
189 were most likely filled with a fluid. Several analogous grains are observed intergrown with iron nitride,
190 Fe_3N (Fig. 1a). Chemical compositions of these oxides, calculated from the EDX spectra and represented
191 in Table 2, are variable. Two of them (from foil #4588 and grain 'd' from foil #4592) are Cr-Mn-Fe
192 oxides with minor admixtures of V (1.27-3.38 at.%) and Si (1.35-1.85 at.%). Two others (grains 'b' and
193 'c' from foil #4592) are Mn-Fe oxides; grain 'c' contains as well 23.07 at.% Cr. Grain 'b', according to
194 the electron diffraction data, has a cubic structure (possibly, retrograde). Grains 'c' and 'd' are
195 orthorhombic, most likely with a CF structure, known for xieite, $FeCr_2O_4$, in meteorites (Chen et al. 2003
196 2008) and Mg-xieite, $MgCr_2O_4$, from a lower-mantle xenolith, where it associates with carbonitrides
197 (Kaminsky et al. 2015). These grains have the potential to be Mn-rich xieite and demonstrate a wide
198 compositional range of post-spinel oxides within the lower mantle.
199
200 **Discussion**
201
202 **Iron carbides, nitrides and intermediate compounds in the natural environment**
203

The most widely known iron carbide is ***cohenite***, Fe_3C, which was discovered in the early nineteenth century. It was first recognized in the diamond-bearing, iron meteorite, Magura (Slovakia) in the 1840s and was named after Professor E.M. Cohen (Weinschenk 1889). Since its discovery, cohenite has been identified in many other iron meteorites (Buchwald 1975). In addition to meteorites, cohenite was found as an inclusion in monocrystalline diamond from the 23rd Party Congress kimberlite, Yakutia (Bulanova and Zayakina 1991). Subsequently, cohenite has also been identified in a polymineralic diamond aggregate (boart) from pipe Venetia, in the Republic of South Africa, where cohenite in association with native iron and troilite was included in garnet (Jacob et al. 2004). More recently, cohenite has been reported upon in diamond from the Jagersfontein pipe, South Africa, where it associates with other Fe-Cr (Cr up to 15 wt. %) and Fe-Ni (Ni up to 9.3 wt. %) carbides (Jones et al. 2008). In addition to its presence in inclusions within kimberlitic diamond, cohenite was met in association with diamond in ophiolitic chromitite from Luobasha, Tibet, along with another iron carbide, ***yarlongite*** $(Fe,Cr,Ni)_9C_4$ (Shi et al. 2009). Besides diamond parageneses in kimberlite and ophiolite, cohenite + native iron + graphite associations are known from basaltic rocks found at Bühl, near Kassel, in Germany (Irmer 1920) and on Disko Island, Greenland (Goodrich and Bird 1985; Ulff-Møller 1985). Cohenite was further reported on in lunar rocks collected in almost all of the Apollo missions (Goldstein et al. 1976) and in lunar soil recovered during various lunar missions (Barsukov and Tarasov 1982). As well as these occurrences in the natural environment, cohenite as 'cementite' is well-known from and has been studied in metallurgy since the 1890s.

In addition to cohenite and yarlongite, another iron carbide ***haxonite*** $(Fe,Ni,Co)_{23}C_6$ was identified in the Toluca (Mexico) and Canyon Diablo (USA) iron meteorites by Scott (1971), as well as in several other iron meteorites (Buchwald 1975). It occurs as a minor accessory in meteorites that also contain cohenite. Both cohenite and haxonite, in meteorites, are frequently found to have decomposed to ferrite and graphite, reflecting thermodynamic instability for these minerals under atmospheric pressure and temperature conditions (Buchwald 1975).

In 1854 the iron carbide, '***chalypite***' was identified by Forchhammer (1861), as a leading constituent of the Niakornak, Greenland, iron 'meteorite'; it was thereafter named by Shepard (1867). Shepard (1867), in his classification of meteorites, distinguished a special group of iron meteorites as 'chalypitic', or 'steel-like' (from the Greek word χαλυψ = steel); the principal mineral constituent of these meteorites was termed 'chalypite'. In fact, there is no such 'Niakornak meteorite'. The name Niakornak does not exist in any meteorite database. The reason for this is that "iron", identified during the mid-19th century investigations of rock from near the Niakornak location on the Island of Disko in western Greenland (also known as 'Ovifak irons'), was initially considered as an iron meteorite (Nordenskiöld 1871), and only later was this recognised as terrestrial native iron (Steenstrup 1875). Prof. V. Buchwald considers the Niakornak iron as "a stray member, a loose boulder of the Ovifak occurrence" (V. Buchwald, personal communication, March 1 2012); he has characterized it in his paper on the use of iron by the Eskimos in Greenland (Buchwald 1992). Most likely, the 'Niakornak meteorite' specimen, studied by Forchhammer (1861), was a part of the 9.7-kg block, received in 1847 by H. Rink from Eskimos at that locality, and originally from the Ovifak locality on the southern coast of Disko Island (Nordensköld, 1870; Buchwald 1975). The exact chemical formula of the first finds of chalypite is unclear. In the first analyses from the Niakornak iron, carbon content was documented at between 7.23-11.06 wt. %, "which would indicate the formula of Fe_2C for this species" (Shepard, 1867). [In all later references (Weinschenk, 1889; Strunz 1978) this mineral has a quoted formula of Fe_2C, although Shepard himself, considering uncertainty in the carbon determination, indicated chalypite as Fe*C*. Indeed, in those first analyses, the F/C ratio varies from 1.74 to 2.75, which may include yarlongite and Fe_7C_3.] Chalypite has not subsequently been identified in any meteorite following its initial discovery (probably because all iron carbides found in meteorites have been considered *a priori* to be cohenite; many of them were not analyzed). This absence provided grounds for Buchwald (1975) to consider the mineral as misinterpreted cohenite; later he offered to delete this mineral from his list (Buchwald 1977). This suggestion, in our opinion, was premature because in both our previous works (Kaminsky and Wirth

2011; Kaminsky et al. 2015) and the current study, such a compound has been identified with Fe/C ratios at 1.95-2.14 and compositions from Fe_2C to Fe_2N.

In our study of iron carbides from Juina diamonds in Brazil we successfully identified all earlier known iron carbides with the exception of yarlongite, as well as possible Fe_5C_3 with Fe/C = 1.65-1.77 and $Fe_{10}C_3$ with Fe/C = 3.33-3.59 (Kaminsky and Wirth 2011). We also suggested that some of the 'chalypite' grains may in fact belong to the Fe_7C_3 stoichiometry. In this work, we demonstrate the presence of orthorhombic Fe_7C_3 as an inclusion in Juina diamond. Most of these iron carbides do not indicate a significant admixture of nitrogen. However, among Fe_5C_3 and Fe_7C_3 grains, ***nitrocarbide*** varieties with N/(C+N) ratio of 0.19-0.24 and 0.27, respectively, were identified. Subsequently nitrocarbides ***and carbonitrides***, $Fe_2(N,C)$ and $Fe_5(N,C)_2$ with 12.8-18.42 at.% N and N/(N+C) = 0.37-0.60 were identified in a lower-mantle microxenolith (Kaminsky et al. 2015).

A summary of carbide-nitride compounds found in the natural environment to date is presented in Table 3 and Fig. 6. These demonstrate a wide field of compositions from pure carbide to pure nitride. Such series of Fe, Co, Ni, Cr and Mn carbides are well studied in technical applications. They belong to so-called intermediate transition-metal carbides, which share features with both the interstitial and the salt-like carbides. Like the interstitial carbides, iron carbides are metal-like compounds that have no ion connection in their crystal lattice; in their structures, carbon atoms occupy interstices between closely packed metal atoms. Different positions of metal atoms in a crystal lattice lead to multiple stoichiometries, such as $M_{23}C_6$, $M_{10}C_3$, M_3C, M_5C_2, M_7C_3, M_9C_4, M_2C, M_5C_3, M_3C_2, M_4C_3, MC, MC_2 with variable (but fixed for each stoichiometry) M/C ratios (Kosolapova 1971; Cottrell 1995). We suggest that the number of N-containing high-pressure natural compounds, particularly from meteorites and inclusions in diamond would be greater if all samples were analyzed for nitrogen.

Depth of origin of Fe_7C_3 and the observed iron nitrides

Iron carbides are stable over a wide range of *P-T* conditions. In metallurgy, various iron carbides occur at ambient conditions. However, detailed studies of Fe-C system under high pressure conditions revealed correlations between pressure of crystallization and the composition of iron carbides. Of particular interest is the Fe_7C_3 compound, which was not identified in the natural environment until recently. High-pressure experiments on the Fe-C system have shown that at pressures above 135 GPa, Fe_7C_3 forms an eutectic relation with Fe (Lord et al. 2009). At 130-135 GPa pressure conditions, Fe_7C_3 is the first iron carbide to crystallize in association with diamond; native iron and diamond associate with Fe_7C_3 in the subsolidus (Fig. 7). This implies that Fe_7C_3 might be stabilized under core and D" layer conditions (Lord et al. 2009; Nakajima et al. 2009). Only at lower pressure conditions, may cohenite and other iron carbides join this association.

In our studied diamond sample from the Juina area (foil #4588), Fe_7C_3 is the only iron carbide phase. Fe_7C_3 associates with nitrides in diamond, and we consider this as evidence of very high-pressure conditions during the formation of this assemblage, most likely at ~130 GPa, i.e. within or near the D" layer, maybe even at the core-mantle boundary, enriched in metals. The C-N-Fe system may be, in this case, the diamond-forming medium, in which nitrogen partitions into metals, forming nitrides. At such conditions nitrides, in particular Fe_3N act as catalysts for diamond formation (Bordzov et al. 2002).

Earlier we found, in the same diamond sample, mineral inclusions of the carbonatitic association: nyerereite, nahcolite, calcite, and others (Kaminsky et al. 2009a, 2015; Wirth 2009). Considering the origin of the primary carbonatitic association, we concluded that it was formed as a result of low-fractional partial melting of lower-mantle material at the core-mantle boundary (Kaminsky et al. 2016). Hence the origin of the both carbonatitic and nitride-carbonitride associations belong to the same lowermost mantle zone; and their coexistence in one sample seems logic.

The presence of Fe_7C_3 in the deep Earth explains seismological data in this region. Until recently, the enigmatic region of low shear wave velocity in the inner core (Dziewonski and Anderson 1981) remained unexplained with consideration to the pure iron composition of this part of the Earth's interior. Partial melting of the outer layer of the inner core, resulting from heat flux variations at the core-mantle

boundary, was suggested as a cause for this effect (Gubbins et al. 2011). Another explanation can be offered with respect to the presence of Fe_7C_3 in the inner core. The calculated density for Fe_7C_3 provides a good explanation for the inferred density of the Earth's inner core, obtained from seismological observations (Nakajima et al. 2011; Chen et al. 2012). A further density change may also be explained by the iron high spin → low spin transition, which produces remarkable shear softening in the low-spin Fe_7C_3 and may reproduce the obtained V_s value for the inner core (Chen et al. 2014). In addition, partial melting of the outer layer in the inner core was unable to explain the high Poisson's ratio of the inner core, which is practically uniform throughout the entire inner core. The presence of Fe_7C_3, which has a Poisson's ratio similar to that of the Earth's inner core, however, can explain it well. Thus, the presence of Fe_7C_3 provides an explanation for all anomalous elastic properties of the Earth's core (Prescher et al. 2015).

In addition to pure Fe_7C_3, one of the earlier recognised and studied grains, with a fully stoichiometric Fe_7C_3 ratio, that of Fe/(C+N) = 2.32, has a significant admixture of nitrogen, N = 8.13 at.%, i.e. N/(C+N) = 0.27(Kaminsky and Wirth 2011). The existence of nitrogen-containing $Fe_7(C,N)_3$ compounds may help to solve another perceived problem, because the presence of iron nitrides in the D″ layer is closely related to their suggested presence in the core (Adler and Williams 2005). Two iron nitrides, cubic γ-Fe_4N (known from iron meteorites as roaldite) and the hexagonal ε-Fe_7N_3 are known to be stable at high pressures. The experimental study of the Fe-N system demonstrates that Fe_7N_3 with its hexagonal close-packed structure is more stable than cubic close-packed roaldite, Fe_4N, at conditions thought to operate in the inner core (Adler and Williams 2005). In this case, the calculated inner core density corresponds to the mixture of Fe_7N_3 + 8Fe. The elastic parameters of ε-Fe_7N_3 are indistinguishable from those of ε-Fe, hence Fe_7N_3 fits the PREM not worse than Fe_7C_3.

The presence of Fe_7N_3 in the inner core solves another enigma that is anisotropy in this layer. It is well established that the inner core exhibits significant anisotropy, with *P*-wave velocities along the polar axis ~3 % faster than for the equatorial plane (Oreshin and Vinnik 2004 and references therein). Several

hypotheses were offered to explain this, but none of them seems satisfactory (Vocadlo 2009) with the exception of the anisotropic features of Fe_7N_3. The anisotropy of ε-Fe_7N_3 is greater than of pure ε-Fe: *a* axis of ε-Fe_7N_3 is more compressible than the *c* axis, with the difference at approximately 6.4 % (Adler and Williams 2005), while pure ε-Fe has only a 3.5 % difference between *a* axis and *c* axis (Stixrude and Cohen 1995). This allows for the consideration of Fe_7N_3 as a better material to satisfy the observed anisotropy in the inner core (Morelli et al. 1986).

These features make ε- Fe_7N_3 the most likely component of the core and explain the presence of nitrides in the D″ layer as a result of any core-mantle interaction. The Fe_3N structure permits a broad range of stoichiometries because of the large number of unoccupied sites, from near Fe_2N to near Fe_4N (Jack 1952). Thus various iron nitrides may be present in the deep Earth, in addition to those identified in this work, Fe_2N and Fe_3N.

Nitrogen in the deep Earth

Nitrogen, along with other elements lighter than Fe and Ni, such as C, O, Si, H and S comprise together approximately 5-10 % of the core's mass (Stixrude et al. 1997; McDonough 2014). Suggested concentrations of nitrogen in the core vary greatly from 3-90 ppm (Jacobs et al. 1995; Zhang and Yin 2012; McDonough 2014) to 5,000 ppm (Sugiura 1998; Adler and Williams 2005).

Reported in this work, nitrides and carbonitrides are not the only nitrogen-containing compounds in the deep Earth. Numerous inclusions of nitrogen have been identified in lower-mantle diamond (Kaminsky et al. 2013; Kagi et al. 2016; Rudloff-Grund et al. 2016). Diamond itself contains nitrogen; over 90% of mantle-derived diamonds contain as much as 3500 ppm of nitrogen as the primary impurity (Cartigny, 2005). These observations imply that nitrogen may after all not be "a useless element in mantle geochemistry" (Cartigny and Marty 2013) but quite the reverse; nitrogen may play a great role in both the core and the mantle, and the existing estimates for nitrogen concentration in this area need

355 reconsideration. It may occur that the 'missing nitrogen' resides in the deep Earth, and the value of bulk
356 Earth/carbonaceous chondrite ratio equal to 0.11 % (Marty 2012) is not a valid estimate. More likely, an
357 estimate for the nitrogen concentration in the core falls close to the one determined in taenite from iron
358 meteorites (i.e., 100-10,000 ppm; Sugiura 1998) and, in the mantle, close to the one established in work
359 on chondrites (e.g., 345-3180 ppm; Kerridge 1985; McDonough and Sun 1995; Palme and O'Neil 2004).
360 Accepting a conventional concentration of nitrogen in the core at 5,000 ppm (Adler and Williams
361 2005) and the partition coefficient between metal core and mantle material at 40 (McDonough 2014), and
362 considering the total core mass as 1.972×10^{27} g and mantle mass as 4.043×10^{27} g (Yoder 1995), the
363 total mass of nitrogen in the core could be $9{,}660 \times 10^{21}$ g and in the bulk mantle 505×10^{21} g, comprising
364 accordingly 94.97 % and 4.97 % of the total nitrogen in the Earth. In this case, the total nitrogen
365 concentration in bulk Earth is 17.03 ppm, which fully corresponds (with an error of ± 2 %) to the
366 concentration of nitrogen as determined in chondrite meteorites. These calculations may be considered as
367 only the first approximation because the exact concentrations of nitrogen and partition values depend on
368 pressure, the oxygen fugacity (fO_2), the form of dissolution of nitrogen in metal and silicate melts, and
369 other factors (Bouhifd et al. 2010; Kadik et al. 2011 2013; Roskosz et al. 2013; Dalou et al. 2016; Li et al.
370 2016). However, the presented data witness that the core and deep mantle are the plausible major
371 reservoirs of nitrogen in the Earth, and that the concentration of nitrogen in the Earth is similar to that of
372 other planets and asteroids.
373
374 **Implications**
375
376 Iron nitrides and carbonitrides, along with iron carbides and native iron form inclusions in lower-mantle
377 diamonds. These phases associate with iron carbide, Fe_7C_3, and silicon carbide, SiC. We suggest their
378 origin lies in the lowermost mantle as the result of the infiltration of liquid metal, containing light
379 elements, from the outer core into the D" layer, with the formation of the phase association: native Fe^0 +
380 iron nitrides, carbides and transitional compounds + silicon carbide.

We further suggest that the described and previous finds of nitrides, carbonitrides and nitrocarbides, along with existence of nitrogen inclusions in diamond, indicate the important role of nitrogen in the deep Earth and are a key for the identification of 'missing nitrogen' in the Earth's core. The concentration of nitrogen in the core is ~0.5 wt.%. The total nitrogen balance in the core is $\sim 1 \times 10^{24}$ g, which is several magnitudes higher than the total nitrogen budget in other parts of the Earth (Miyazaki et al. 2004). At the core/mantle boundary and in the inner core, nitrogen forms trivalent N^{3-} groups during crystallization in nitrocarbides and carbonitrides as a result of core/mantle interaction. ε-Fe_3N is the most likely nitride phase in the core, where the iron atoms are arranged in a distorted hexagonal closest packed structure, similar to ε-Fe (Jacobs et al. 1995).

Light elements (C, N, Si), forming with iron a series of native Fe^0, iron nitrides-carbonitrides-nitrocarbides-carbides and silicon carbide, infiltrate into the D″ layer within Fe-enriched liquid metal migrating from the outer core. Such a process may be the result of the deformation-induced mechanical instabilities at the core-mantle boundary, caused by the accumulation of strain deformations in high stress zones, associated with down-welling material (Petford et al. 2007). This process has its support in experiments with chondrites, in which metallic layers were observed infiltrating silicate chondritic material (Rushmer et al. 2000).

This scenario helps to solve the problem of 'missing nitrogen' in the Earth's nitrogen balance; it demonstrates the presence of the majority of the Earth's nitrogen in the core and the lowermost mantle.

Acknowledgements

The authors thank Anja Schreiber for milling FIB foils from diamond samples and Dr. A. Shiryaev and an anonymous reviewer for their constructive criticism, which helped us to improve the manuscript.

References

406

407 Adler, J.F., and Williams, Q. (2005) A high-pressure X-ray diffraction study of iron nitrides: Implications
408 for Earth's core. Journal of Geophysical Research 110, B01203. DOI: 10.1029/2004JB003103..
409 Barsukov, V.L., and Tarasov, L.S. (1982) Moon rock mineralogy. International Geology Review 26, 238-
410 248.
411 Bergin, E.A., Blake, G.A., Ciesla, F., Hirschmann, M.M., and Li, J. (2015) Tracing the ingredients for a
412 habitable earth from interstellar space through planet formation. Proceedings of the National
413 Academy of Sciences of the U.S.A.112, 8965–8970. DOI: 10.1073/pnas.1500954112.
414 Bouchard, J.P. (1967) Etude structural des carbures des manganeses. Annales de Chimie, vol. 1967, 353 -
415 366.
416 Bouhifd, M.A., Roskosz, M., Jephcoat, A.P., and Mysen, B.O. (2010) Nitrogen solubility in a molten
417 assemblage of an (Fe,Ni) alloy and a CI chondritic silicate up to 18 GPa. Geochimica et
418 Cosmochimica Acta 74 (12S), A109.
419 Buchwald, V.F. (1975) Handbook of iron meteorites, their history, distribution, composition, and
420 structure. Volume 1. Tempe & Berkeley, Center for Meteorite Studies, and University of California
421 Press, 243 pp.
422 Buchwald, V.F. (1977) Mineralogy of iron meteorites. Philosophical Transactions of the Royal Society of
423 London. Series A, Mathematical and Physical Sciences 286, 453-491.
424 Buchwald, V.F. (1992) On the use of iron by the Eskimos in Greenland. Materials Characterization 29
425 (2), 139-176.
426 Bulanova, G.P., and Zayakina, N.V. (1991) Graphite – iron – cohenite assemblage in the central zone of
427 diamond from 23rd Party Congress kimberlite. Doklady Akademii Nauk SSSR 317, 706–709. (in
428 Russian).
429 Busigny, V., and Bebout, G.E. (2013) Nitrogen in the silicate Earth: Speciation and isotopic behavior
430 during mineral–fluid Interactions. Elements 9, 353-358.

Capitani, G. C., Di Pierro, S., and Tempesta, G. (2007) The 6H-(SiC) structure model: further refinement from SCXRD data from a terrestrial moissanite. American Mineralogist 92, 403 – 407.

Cartigny, P. (2005) Stable isotopes and the origin of diamond. Elements 1(2), 79-84.

Cartigny, P., Marty, B. (2013) Nitrogen isotopes and mantle geodynamics: The emergence of life and the atmosphere–crust–mantle connection. Elements 9, 359-366.

Chen, B., Gao, L., Lavina, B., Dera, P., Alp, E.E., and Li, J. (2012) Magneto-elastic coupling in compressed Fe_7C_3 supports carbon in Earth's inner core. Geophysical Research Letters 39, L18301. DOI: 10.1029/2012GL052875.

Chen, B., Li, Z., Zhang, D., Liu, J., Hu, M.Y., Zhao, J., Bi, W., Alp, E.E., Xiao, Y., Chow, P., and Li, J. (2014) Hidden carbon in Earth's inner core revealed by shear softening in dense Fe_7C_3. Proceedings of the National Academy of the U.S.A. 111 (50), 17755-17758. DOI: 10.1073/pnas.1411154111.

Chen, M., Shu, J., Mao, H.-k., Xie, X., and Hemley, R.J. (2003) Natural occurrence and synthesis of two new postspinel polymorphs of chromite. Proceedings of the National Academy of the U.S.A. 100, 14651–14654.

Chen, M., Shu, J., and Mao, H.-k. (2008) Xieite, a new mineral of high-pressure $FeCr_2O_4$ polymorph. Chinese Science Bulletin 53, 3341-3345.

Cottrell, A.H. (1995) Chemical bonding in transition metal carbides. Institute of Metals, London, 97 pp.

Dalou, C., Hirschmann, M.M., von der Handt, A., Mosenfelder, J., and Armstrong, L.S. (2016) Nitrogen and carbon fractionation during core–mantle differentiation at shallow depth. Earth and Planetary Science Letters 458, 141–151. DOI: 10.1016/j.epsl.2016.10.026.

Dziewonski, A., and Anderson, D. (1981) Preliminary reference Earth model. Physics of Earth and Planetary Interiors. 25, 297-356. DOI: 10.1016/0031-9201(81)90046-7.

Forchhammer, J.G. (1861) Fortegnelse over de i Universitetets Mineralsampling opbevarede Meteoriter. Oversigt over det Kongelige Danske Videnskabernes Selskabs Forhandlinger, Copenhagen, June, 225-229.

Goldblatt, C., Claire, M.W., Lenton, T.M., Matthews, A.J., Watson, A.J., and Zahnle, K.J. (2009)

457 Nitrogen-enhanced greenhouse warming on early Earth. Nature Geoscience 2, 891-896.
458 Goldstein, G.I., Hewins, R.H., and Romig, A.D., Jr. (1976) Carbides in Lunar soils and rocks. Abstracts
459 of the Lunar and Planetary Science Conference 7, 310-312.
460 Goodrich C.A., and Bird J.M. (1985) Formation of iron-carbon alloys in basaltic magma at Uivfaq, Disko
461 Island; the role of carbon in mafic magmas. Journal of Geology 93, 475–492.
462 Gubbins, D., Sreenivasan, B., Mound, J., and Rost, S. (2011) Melting of the Earth's inner core. Nature
463 473, 361-363. DOI: 10.1038/nature10068.
464 Goldstein, G.I., Hewins, R.H., and Romig, A.D., Jr. (1976) Carbides in Lunar soils and rocks. Abstracts
465 of the Lunar and Planetary Science Conference 7, 310-312.
466 Goodrich C.A., and Bird J.M. (1985) Formation of iron-carbon alloys in basaltic magma at Uivfaq, Disko
467 Island; the role of carbon in mafic magmas. Journal of Geology, 93, 475–492.
468 Hirschmann, M.M. (2016) Constraints on the early delivery and fractionation of Earth’s major volatiles
469 from C/H, C/N, and C/S ratios. American Mineralogist 101, 540–553. DOI: 10.2138/am-2016-
470 5452.
471 Hutchison, M.T., Cartigny, P., and Harris, J.W. (1999) Carbon and nitrogen compositions and physical
472 characteristics of transition zone and lower mantle diamonds from São Luiz, Brazil. In: Gurney,
473 J.J., Gurney, J.L., Pascoe, M.D. and Richardson, S.H. (eds), Proceedings of the VIIth International
474 Kimberlite Conference, vol. 1, Red Roof Design, Cape Town, p. 372-382.
475 Irmer, W. (1920) Der Basalt des Bühls bei Kassel und seine Einschlüsse von Magnetit, Magnetkies und
476 gediegen Eisen. Abhandlungen der Senckenbergischen Naturforschenden Gesellschaft 13, 91–108.
477 Jack, K.H. (1952) The iron-nitrogen system: The crystal structures of ε-phase iron nitrides. Acta
478 Crystallographica 5, 404-411.
479 Jacob, D.E., Kronz, A., and Viljoen, K.S. (2004) Cohenite, native iron and troilite inclusions in garnets
480 from polycrystalline diamond aggregates. Contributions to Mineralogy and Petrology 146, 566–
481 576.

Jacobs, H., Rechenbach, D., and Zachwieja, U. (1995) Structure determination of γ-Fe_4N and ε-Fe_3N. J. Alloys and Compounds 277, 10–17.

Jones, A.P., Dobson, D., Wood, I., Beard, A.D., Verchovsky, A., and Milledge, H.J. (2008) Iron carbide and metallic inclusions in diamonds from Jagersfontein. 9th International Kimberlite Conference, Extended Abstract No. 9IKC-A-00360, 3 pp.

Kadik, A.A., Kurovskaya, N.A., Ignat'ev, Yu.A., Kononkova, N.N., Koltashev, V.V., and Plotnichenko, V.G. (2011) Influence of oxygen fugacity on the solubility of nitrogen, carbon, and hydrogen in $FeO–Na_2O–SiO_2–Al_2O_3$ melts in equilibrium with metallic iron at 1.5 GPa and 1400 C. Geochemistry International 49, 429–438.

Kadik, A.A., Litvin, Yu.A., Koltashev, V.V., Kryukova, E.B., Plotnichenko, V.G., Tsekhonya, T.I., and Kononkova, N.N. (2013) Solution behavior of reduced N–H–O volatiles in $FeO–Na_2O–SiO_2–Al_2O_3$ melt equilibrated with molten Fe alloy at high pressure and temperature. Physics of the Earth and Planetary Interiors 214, 14–24.

Kagi, H., Zedgenizov, D.A., Ohfuji, H., and Ishibashi, H. (2016) Micro- and nanoinclusions in a superdeep diamond from São Luiz, Brazil. Geochemistry International 54(10), 834-838.

Kaminsky, F.V., and Wirth, R. (2011) Iron carbide inclusions in lower-mantle diamond from Juina, Brazil. Canadian Mineralogist 49(2), 555-572. DOI: 10.3749/canmin.49.2.555.

Kaminsky, F., Wirth, R., Matsyuk, S., Schreiber, A., and Thomas, R. (2009a) Nyerereite and nahcolite inclusions in diamond: Evidence for lower-mantle carbonatitic magmas. Mineralogical Magazine 73 (5), 797-816. DOI: 10.1180/minmag.2009.073.5.797.

Kaminsky, F.V., Khachatryan, G.K., Andreazza, P., Araujo, D., and Griffin, W.L. (2009b) Super-deep diamonds from kimberlites in the Juina area, Mato Grosso State, Brazil. Lithos112S(2), 833-842. DOI: 10.1016/j.lithos.2009.03.036.

Kaminsky, F.V., Wirth, R., and Schreiber, A. (2013) Carbonatitic inclusions in Deep Mantle diamond from Juina, Brazil: New minerals in the carbonate-halide association. Canadian Mineralogist 51 (5), 447-466. DOI: 10.3749/canmin.51.5.669.

508 Kaminsky, F.V., Wirth, R., and Schreiber, A. (2015) A microinclusion of lower-mantle rock and some
509 other lower-mantle inclusions in diamond. Canadian Mineralogist 53(1), 83-104. DOI:
510 10.3749/canmin.1400070.
511 Kaminsky, F.V., Ryabchikov, I.D., and Wirth, R. (2016) A primary natrocarbonatitic association in the
512 Deep Earth. Mineralogy and Petrology 110(2-3), 387-398. DOI: 10.1007/s00710-015-0368-4.
513 Kerridge, J.F. (1985) Carbon, hydrogen and nitrogen in carbonaceous chondrites: Abundance and isotopic
514 compositions in bulk samples. Geochimica et Cosmochimica Acta 49, 1707-1714.
515 Kosolapova, T.Ya. (1971) Carbides: Properties, Production, and Applications. Plenum Press, New York,
516 N.Y., 298 pp.
517 Leineweber, A., Jacobs, H., Huening, F., Lueken, H., and Kockelmann, W. (2001) Nitrogen ordering and
518 ferromagnetic properties of ε-(Fe_3N_{1+x} ($0.10 \leq x \leq 0.39$) and ε-$Fe_3(N_{0.80}C_{0.20})_{1.38}$. Journal of Alloys
519 and Compounds 316, 21-38.
520 Li, Y., Wiedenbeck, M., Shcheka, S., and Keppler, H. (2013) Nitrogen solubility in upper mantle
521 minerals. Earth and Planetary Science Letters 377, 311-323.
522 Li, Y., Marty, B., Shcheka, S., Zimmermann, L., and Keppler, H. (2016) Nitrogen isotope fractionation
523 during terrestrial core–mantle separation. Geochemical Perspectives Letters 2, 138–147.
524 Lord, O.T., Walter, M.J., Dasgupta, R., Walker, D., and Clark, S.M. (2009) Melting in the Fe–C system
525 to 70 GPa. Earth and Planetary Science Letters, 284, 157–167. DOI: 10.7185/geochemlet.1614.
526 Marty, B. (2012) The origins and concentrations of water, carbon, nitrogen and noble gases on Earth.
527 Earth and Planetary Science Letters 313–314, 56–66. DOI: 10.1016/j.epsl.2011.10.040.
528 McDonough, W.F. (2014) Compositional Model for the Earth's Core. In: Treatise on Geochemistry, 2nd
529 edition. Vol. 3 (Ed. R.W. Carlson), p. 559-576. Elsevier.
530 McDonough, W.F., and Sun, S.-S. (1995) Composition of the Earth. Chemical Geology 120, 223-253.
531 DOI: 10.1016/0009-2541(94)00140-4.
532 Miyazaki, A., Hiyagon, H., Sugiura, N., Hirose, K., and Takahasi, E. (2004) Solubilities of nitrogen and
533 noble gases in silicate melts under various oxygen fugacities: Implications for the origin and

degassing history of nitrogen and noble gases in the Earth. Geochimica et Cosmochimica Acta 68, 387–401.

Morelli, A., Dziewonski, A.M., and Woodhouse, J.H. (1986) Anisotropy of the inner core inferred from PKIKP travel times. Geophysical Research Letters 13, 1545–1548.

Nakajima, Y., Takahashi, E., Suzuki, T., and Funakoshi, K.-i. (2009) "Carbon in the core" revisited. Physics of the Earth and Planetary Interiors 174, 202–211.

Niewa, R., Rau, D., Wosylus, A., Meier, K., Hanfland, M., Wessel, M., Dronskowski, R., Dzivenko, D.A., Riedel, R., and Schwarz, U. (2009) High-pressure, high-temperature single crystal growth, ab initio electronic structure calculation and equation of state of ε- Fe_3N_{1+x}. Chemistry of Materials 21 (2), 392–398. DOI**:** 10.1021/cm802721k.

Nordenskiöld, A.E. (1870) Redogörelse for en expedition till Grönland or 1870. Öfversigt af Svenska Vetenskaps-Akademiens Förhandlinger, Stockholm 27, 1057-1070.

Nordenskiöld, A.E. (1871) Redogörelse for en ekspedition till Grönland 1870. Öfversigt af Svenska Vetenskaps-Akademiens Förhandlinger, Stockholm 28, 973-1082.

Oreshin, S.I., and Vinnik, L.P. (2004) Heterogeneity and anisotropy of seismic attenuation in the inner core. Geophysical Research Letters 31, L02613.

Palme, H., and O'Neill, H.St.C. (2004) Cosmochemical estimates of Mantle Composition. In: Treatise on Geochemistry. Holland, H.D. and Turekian, K.K. (Editors), Elsevier, Amsterdam, The Netherlands. 2, 1-38.

Petford, N., Rushmer, T., and Yuen, D. A. (2007) Deformation- induced mechanical instabilities at the core-mantle boundary. Post-Perovskite, The Last Mantle Phase Transition, 271-287 (AGU 2007).

Prescher, C., Dubrovinsky, L., Bykova, E., Kupenko, I., Glazyrin, K., Kantor, A., McCammon, C., Mookherjee, M., Nakajima, Y., Miyajima, N., Sinmyo, R., Cerantola, V., Dubrovinskaia, N., Prakapenka, V., Rüffer, R., Chumakov, A., and Hanfland, M. (2015) High Poisson's ratio of Earth's inner core explained by carbon alloying. Nature Geoscience 8, 220-223.

559 Rechenbach, D., and Jacobs, H. (1996) Structure determination of ζ-Fe_2N by neutron and synchrotron
560 powder diffraction. Journal of Alloys and Compounds 235 (1), 15–22.
561 Roskosz, M., Bouhifd, M.A., Jephcoat, A.P., Marty, B., and Mysen, B.O. (2013) Nitrogen solubility in
562 molten metal and silicate at high pressure and temperature. Geochimica et Cosmochimica Acta 121,
563 15-28.
564 Rudloff-Grund, J., Brenker, F., Marquardt, K., Howell, D., Schreiber, A., O'Reilly, S.Y., Griffin, W.L.,
565 and Kaminsky, F.V. (2016) Nitrogen-nanoinclusions in milky diamonds from Juina area, Mato
566 Grosso State, Brazil. Lithos 265, 57-67. DOI: 10.1016/j.lithos.2016.09.022.
567 Rushmer, T., Minarik, W. G., and Taylor, G. J. (2000) Physical processes of core formation. Origin of the
568 Earth and Moon, 227-245 (Lunar Planetary Institute and University of Arizona Publishers 2000).
569 Scott, E.R.D. (1971) New carbide $(Fe,Ni)_{23}C_6$, found in meteorites. Nature Physical Sciences 229, 61-62.
570 Shepard, C.U. (1867) New classification of meteorites with an enumeration of meteoric species.
571 American Journal of Science and Arts, Second Series, 43, 22-28.
572 Shi, N., Bai, W., Li, G., Xiong, M., Fang, Q., Yang, J., Ma, Z., and Rong, H. (2009) Yarlongite: A new
573 metallic carbide mineral. Acta Geologica Sinica 83, 52-56.
574 Stixrude, L., and Cohen, R.E. (1995) High-pressure elasticity of iron and anisotropy of Earth's inner core,
575 Science 267 1972– 1975.
576 Stixrude, L., Wasserman, E., and Cohen, R.E. (1997) Composition and temperature of Earth's inner core,
577 Journal of Geophysical Research 102(B11), 24,729–24,739.
578 Steenstrup, K.J.V. (1875) Om de Nordenskiöldske jernmasser og om forekomsten af gediegent jern i
579 basalt. Videnskabelige Meddelelser fra Dansk Naturhistorisk Forening, Copenhagen 7, 284-306.
580 Strunz, H. (1978) Mineralogische Tabellen. 7, unveränderte Auflage, Akademische Verlagsgesellschaft
581 Geest & Portig K.-G., Leipzig, 621 SS.
582 Sugiura, N. (1998) Ion probe measurements of carbon and nitrogen in iron meteorites. Meteoritica and
583 Planetary Sciience 33 (3), 393–409.

584 Tucker, J.M., and Mukhopadhyay, S. (2014) Evidence for multiple magma ocean outgassing and
585 atmospheric loss episodes from mantle noble gases. Earth and Planetary Science Letters 393, 254–
586 265. DOI: 10.1016/j.epsl.2014.02.050.
587 Ulff-Møller, F. (1985) Solidification history of the Kitdlit lens: Immiscible metal and sulphide liquids
588 from a basaltic dyke on Disko, Central West Greenland. Journal of Petrology 26, 64-91.
589 Vocadlo, L. (2009) Mineralogy of the Earth - The Earth's core: Iron and iron alloys. In: Treatise on
590 Geophysics. Mineral Physics, G.D. Price (Ed.). Elsevier, pp. 91-120.
591 Weinschenk, E. (1889) Über einige Bestandtheile des Meteoreisens von Magura, Arva, Ungarn. Annalen
592 des Naturhistorischen Hofmuseums, Wien 4, 93-101.
593 Wirth, R. (2004) Focused Ion Beam (FIB): A novel technology for advanced application of micro- and
594 nanoanalysis in geosciences and applied mineralogy. European Journal of Mineralogy 16, 863-876.
595 Wirth, R. (2009) Focused Ion Beam (FIB) combined with SEM and TEM: Advanced analytical tools for
596 studies of chemical composition, microstructure and crystal structure in geomaterials on a
597 nanometre scale. Chemical Geology 261, 217-229.
598 Wirth, R., Kaminsky, F., Matsyuk, S., and Schreiber, A. (2009) Unusual micro- and nano-inclusions in
599 diamonds from the Juina Area, Brazil. Earth and Planetary Science Letters 286(1-2), 292-303. DOI:
600 10.1016/j.epsl.2009.06.043.
601 Yoder, C.F. (1995) Astrometric and geodetic properties of the Earth and the solar system. In: T.J. Ahrens
602 (ed.) Global Earth Physics: A Handbook of Physical Constants, Vol. AGU Reference Shelf, pp. 1–
603 31. Washington, DC: American Geophysical Union.
604 Zhang, Y., and Yin, Q.-Z. (2012) Carbon and other light element contents in the Earth's core based on
605 first-principles molecular dynamics. Proceedings of the National Academy of the U.S.A. 109(48)
606 19579–19583.

607 **Tables**

608 Table 1. List of samples

Foil #	Major inclusions	Mineral phases
2327	Three grains of iron nitride	Fe_3N trigonal or Fe_2N orthorhombic
2934	Single nitride-graphite grain	Fe_2N orthorhombic
4592	Nitride + graphite	Fe_3N trigonal
	Oxides	(b) (Fe-Mn) cubic
		(c) (Mn-Fe-Cr) orthorhombic
		(d) (Cr-Mn-Fe) orthorhombic
4588	Multiphase: carbonitride + carbide + spinel	$Fe_9(N_{0.8}C_{0.2})_4$ trigonal (host)
		Fe_7C_3 orthorhombic (two lamellae)
		SiC within lamellae
		Cr-Mn-Fe spinel (cubic)

609

610 Table 2. Cation compositions of oxide grains, intergrown with nitride and carbonitride (in at.%)

Element	Foil #4588	Foil #4592		
	Cubic	Oxide "b" Cubic	Oxide "c" Orthorhombic	Oxide "d" Orthorhombic
Cr	60.80	-	23.07	56.17
Mn	29.01	61.00	46.05	25.29
Fe	7.57	37.56	28.09	13.31
V	1.27	-	1.31	3.38
Si	1.35	1.44	1.48	1.85
Total	100.00	100.00	100.00	100.00

611

612 Table 3. Summary on natural iron carbides and nitrides

Theoretic stoichiometries	At. ratio M/(C,N)	Natural compounds		
		Carbides (N/(C+N) < 0.1)	Nitrocarbides (N/(C+N) = 0.1-0.5) and carbonitrides	Nitrides (N/(C+N) > 0.9)

			(N/(C+N) = 0.5-0.9)	
$M_5(C,N)_3$	1.67	Fe_5C_3 (Fe/C = 1.65-1.77) Incl. ##9, 10 in diamond [9]	Fe/(C+N) = 1.65-1.69 N = 0.19-0.24 Incl. ##12, 13 in diamond [9]	
$M_2(C,N)$	2.0	Fe_2C – "chalypite" (1) Niakornak iron [1]; (2) Incl. ##1, 2, 5, 7 in diamond (Fe/C = 1.95-2.14) [9]	Fe/(C+N) = 1.5-2 N/(C+N) = 0.37-0.60 Incl. in diamond [10]	Fe_2N orthorhombic [11]
$M_9(C,N)_4$	2.25	$(Fe,Cr,Ni)_9C_4$ – yarlongite Chromitite [8]	$Fe_9(N_{0.8}C_{0.2})_4$ trigonal N/(C+N) = 0.2 [11]	
$M_7(C,N)_3$	2.33	Fe_7C_3 orthorhombic [11]	Fe/(C+N) = 2.32 N/(C+N) = 0.27 Incl. #14 in diamond [9]	
$M_5(C,N)_2$	2.5		$Fe_5(C,N)_2$ (Fe/(C+N) = 2.52) N/(C+N) = 0.54 Incl. in diamond [10]	
$M_3(C,N)$	3.0	$(Fe,Ni,Co)_3C$ – cohenite (1) Iron meteorites [3]; (2) Lunar soil [4, 5]; (3) Incl. in diamond [3, 7, 9]; (4) Chromitites [8]; (5) Basaltic rocks		Fe_3N trigonal [11]
$M_{10}(C,N)_3$	3.33	$Fe_{10}C_3$ (Fe/C = 3.33-3.59) Incl. ##3, 8, 11 in diamond [9]		
$M_{23}(C,N)_6$	3.83	$(Fe,Ni,Co)_{23}C_6$ – haxonite (1) Iron meteorites [2, 3]; (2) Incl. #6 in diamond (Fe/C = 3.98) [9]		

Captions to figures

Fig. 1. TEM dark-field images of iron nitrides included in diamond #8-103. a – First type. Tabular grain of iron nitride, Fe_3N, intergrown with oxides. Foil #4592. b – Second type. Iron nitride, Fe_2N, resorbed with graphite, which occupies now the major part of the inclusion. Relics of Fe_2N have the same crystallographic orientations, confirming that they belong to a former, single large crystal. Foil #2934.

Fig. 2. EDX spectra of iron nitrides. a – Fe_2N, foil #2934. b – Fe_3N, foil #4592. c – Fe_2N or Fe_3N, foil #2327. The admixture of Si is visible in nitrides from foils ## 2934 and 4592, while it is absent in nitride from foil #2327. Here, and in other EDX spectra, Ga intensity is due to implanted Ga ions during FIB milling; Cu intensity represents copper from the copper grid the foil resides upon.

Fig. 3. HAADF image of iron carbonitride, $Fe_9(N_{0.8}C_{0.2})_4$, with lamellae iron carbide, Fe_7C_3, hosted as an inclusion in diamond. In the lower left part of the image an idiomorphic crystal with spinel-type structure is observed intergrown with carbonitride. The volume below this grain is filled with redeposited Ga and sputtered material; originally it was likely filled with trapped fluid and/or vapour. The outlined square area corresponds to regions for Si and C elemental maps (Fig. 5). Circles show areas for which EDX spectral analyses were determined. Foil #4588.

Fig. 4. Iron carbide lamellae in foil #4588. a - HAADF image of two iron carbide lamellae within the iron carbonitride grain included within diamond. The areas over which EDX analyses were determined are shown in red squares (1 - a brighter contrasted volume within the lamella; 2 – the grey matrix of the lamella). The bright lines in the hosting carbonitride are dislocation lines. b - EEL spectrum of the matrix of the thick lamella. The calculated ratio of Fe/C from this spectrum is 2.46, which is close to the ideal value of 2.33 for Fe_7C_3. c -d - EDX spectra of iron carbide, Fe_7C_3 (c – from matrix without admixture of Si; d – from bright area #1 with a noticeable admixture of Si).

640

641 Fig. 5. Drift-corrected elemental map of the Fe_7C_3 lamellae within carbonitride hosting a cubic grain of
642 SiC. Foil #4588.

643

644 Fig. 6. Compositional ternary plot of natural iron carbides and nitrides from different localities (in at.%).
645 See references in note to Table 3.

646

647 **Supplementary information**

648

649 Supplementary Table 1. Structural characteristics of iron nitride grains

650

651 Supplementary Table 2. Cation compositions of iron nitrides (in at.%).

652

653 Supplementary Table 3. Structural characteristics of iron carbonitride inclusion

654

655 Supplementary Table 4. Structural characteristics of iron carbide

656

657 Supplementary Fig. 1. Electron diffraction pattern from the iron nitride grain in the central part of foil
658 #2327. The diffuse and smeared out diffraction spots suggest a mosaic structure to the grain with a slight
659 misorientation of the individual crystal blocks.

660

661 Supplementary Fig. 2. EDX (a) and EEL (b) spectra of iron carbonitride, $Fe_9(N_{0.8}C_{0.2})_4$. In addition to
662 major Fe, N and C peaks, a smaller peak of Si at ~1.8 keV is present in the EDX spectrum. Foil #4588.

663

Figure 1a

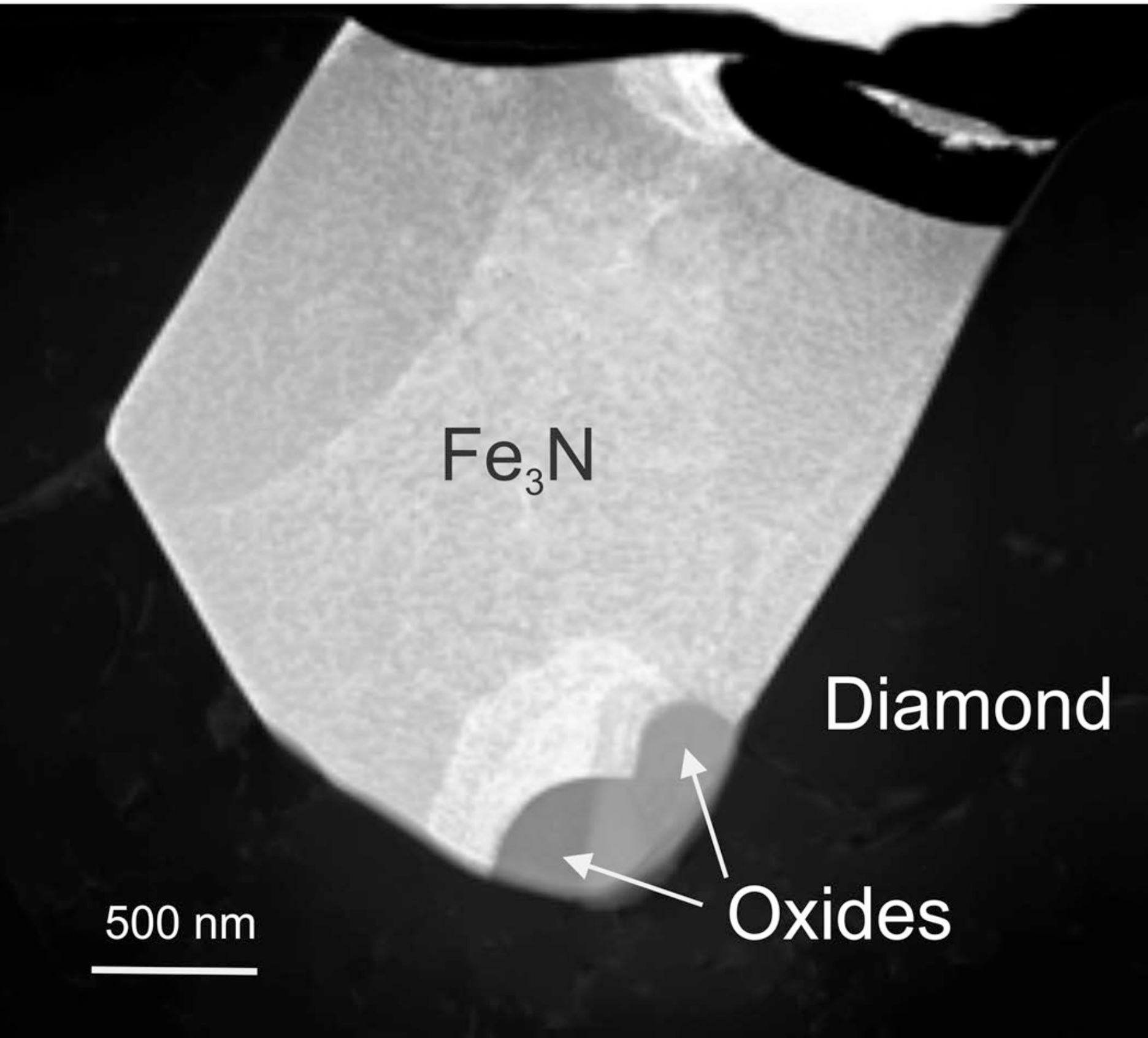

Figure 1b

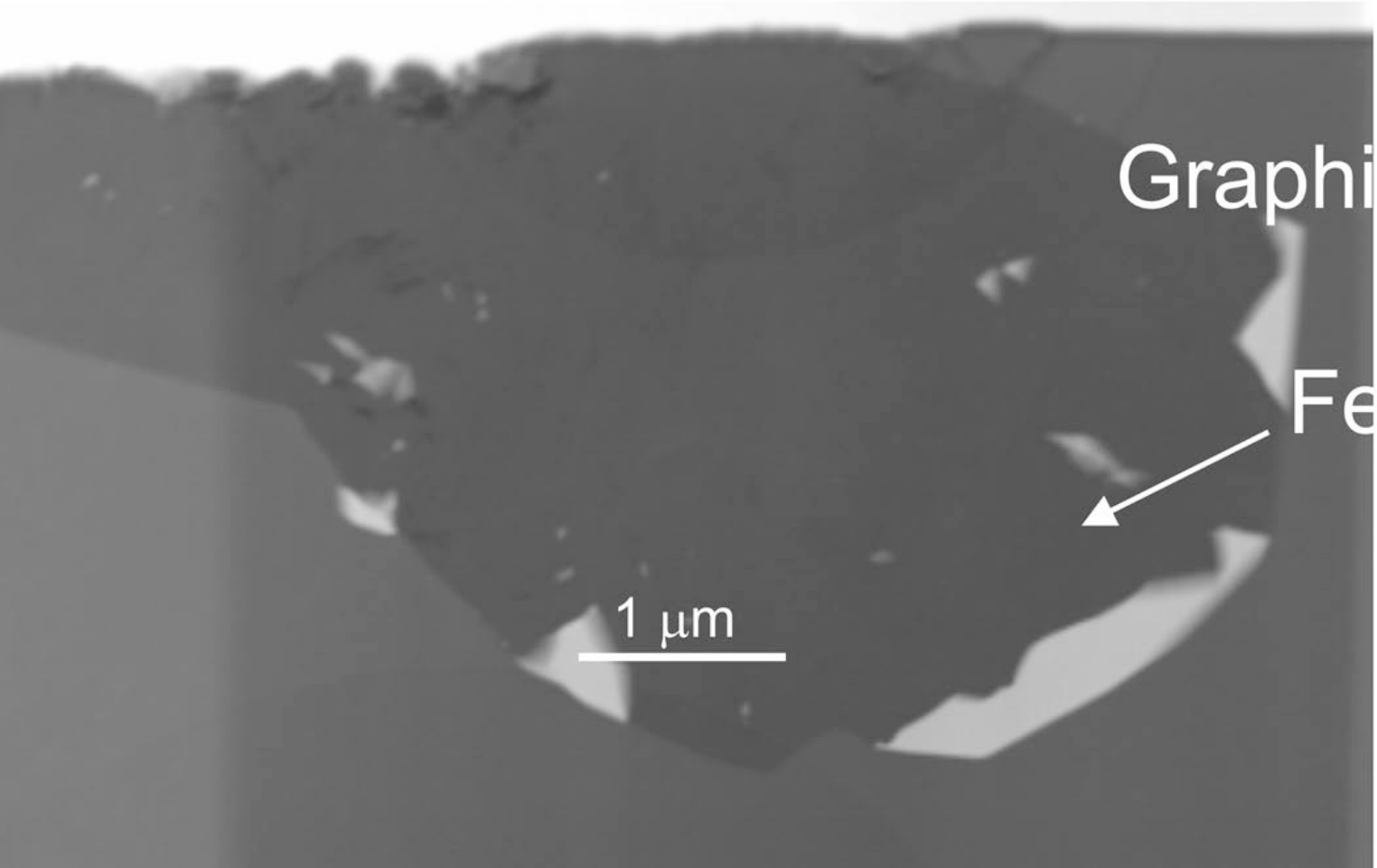

Figure 2

a

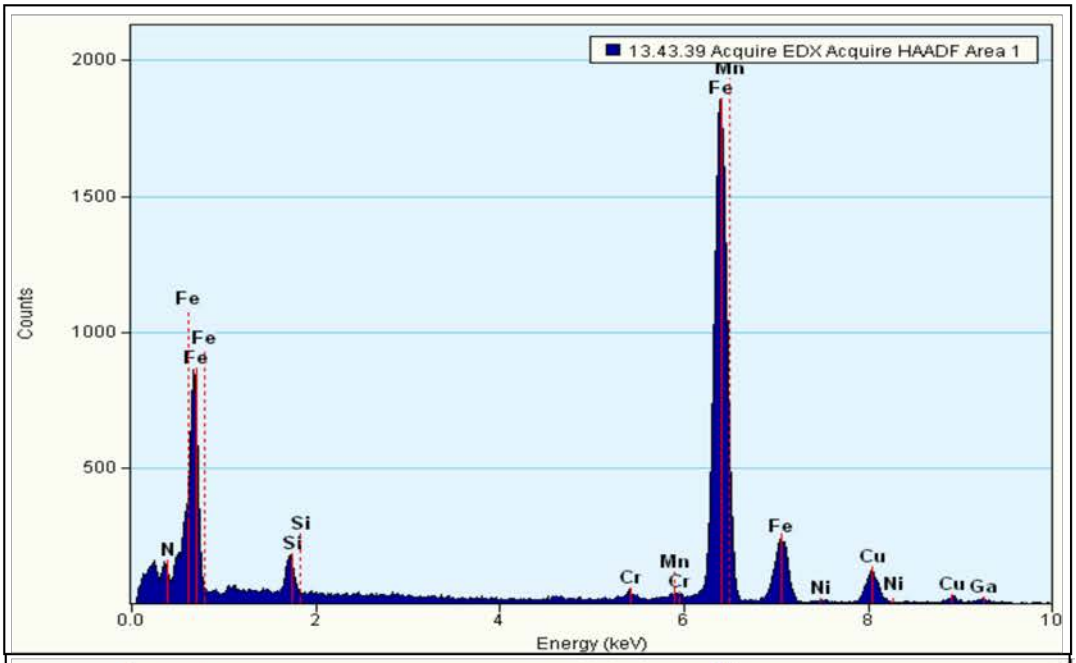
13.43.39 Acquire EDX Acquire HAADF Area 1
Counts
Energy (keV)
Fe
Mn
Si
Cr
Ni
Cu
Ga
N

b

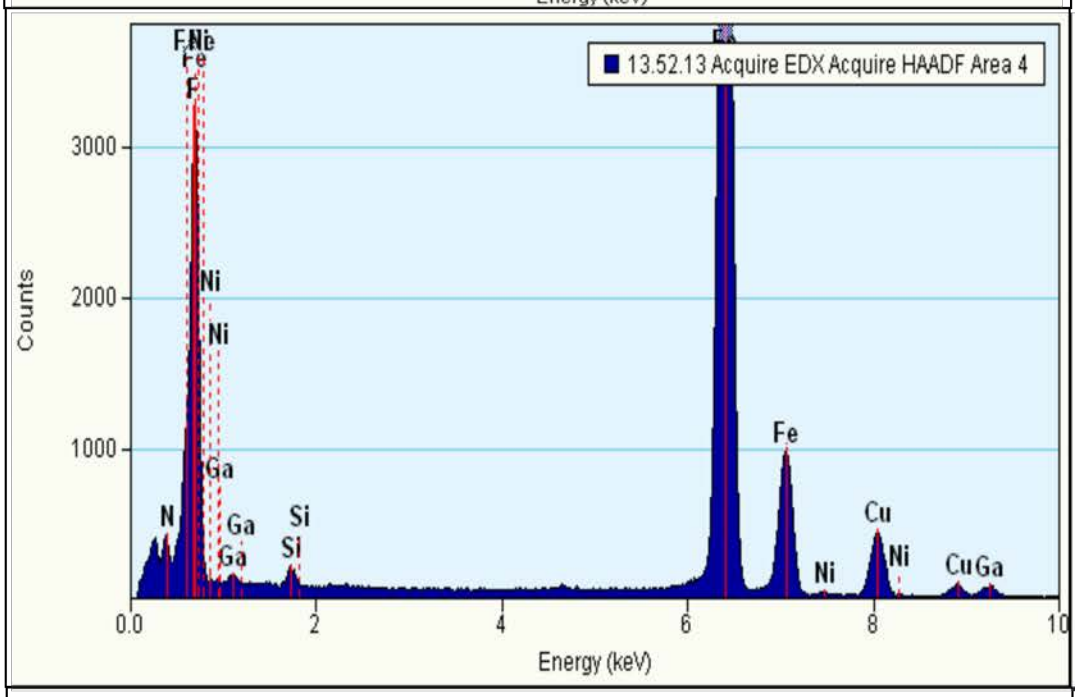
13.52.13 Acquire EDX Acquire HAADF Area 4
Counts
Energy (keV)
Fe
Ni
Ga
Si
N
Cu

c

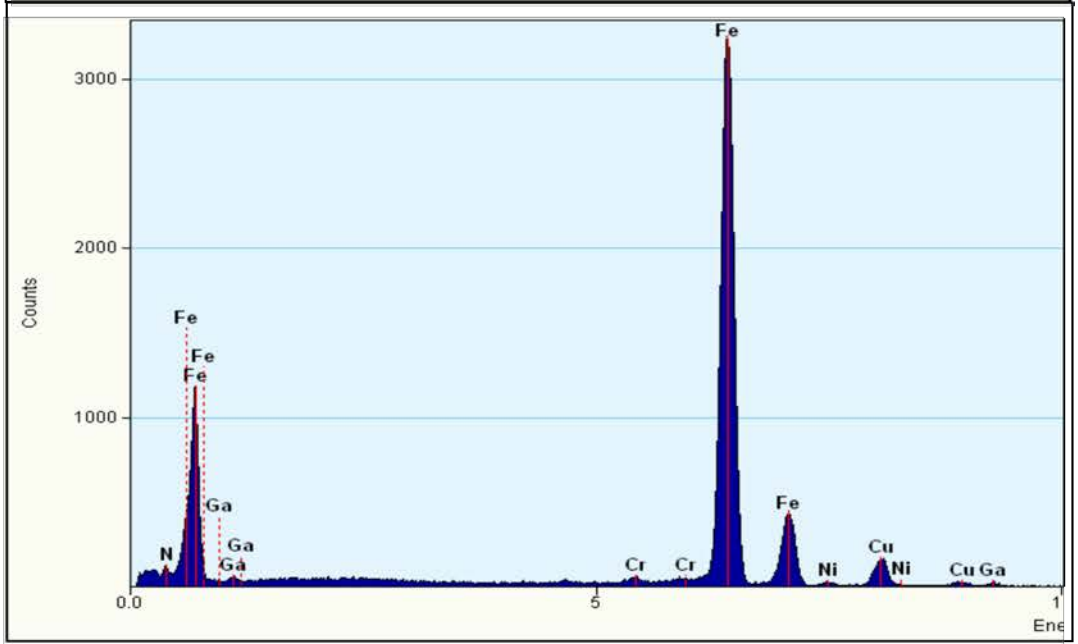
Counts
Fe
Ga
N
Cr
Ni
Cu

Figure 3

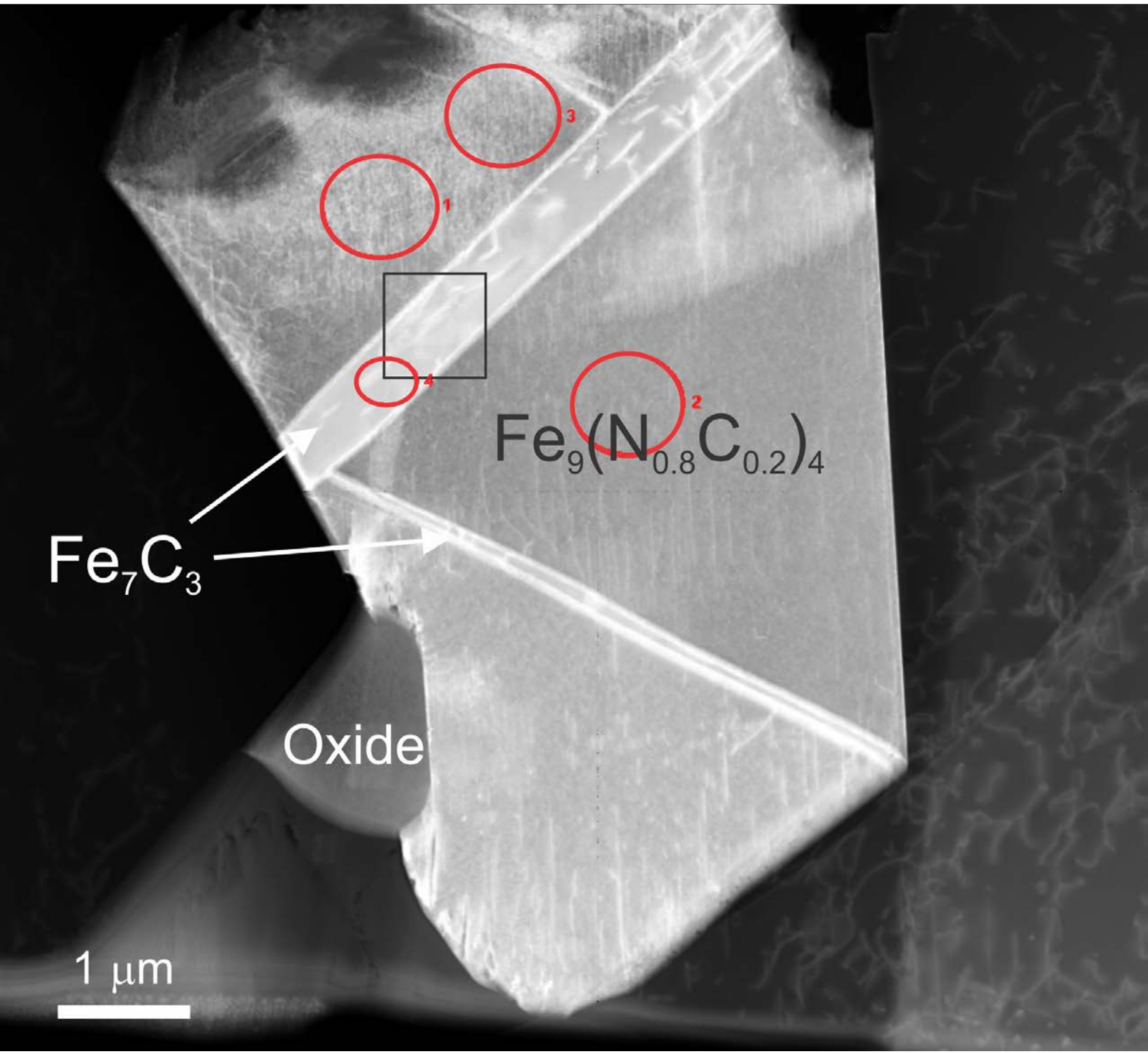

Figure 4

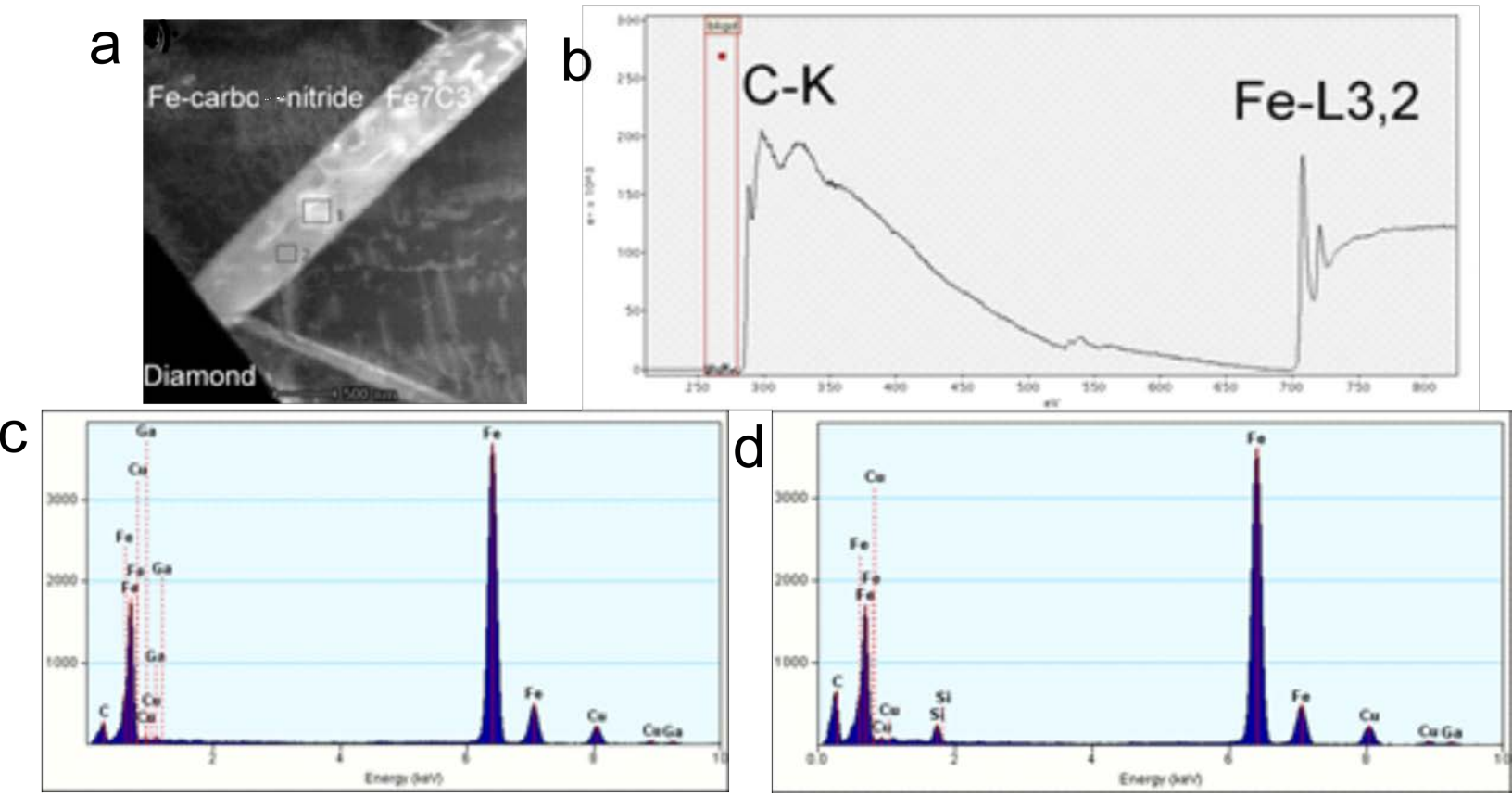

Figure 5a

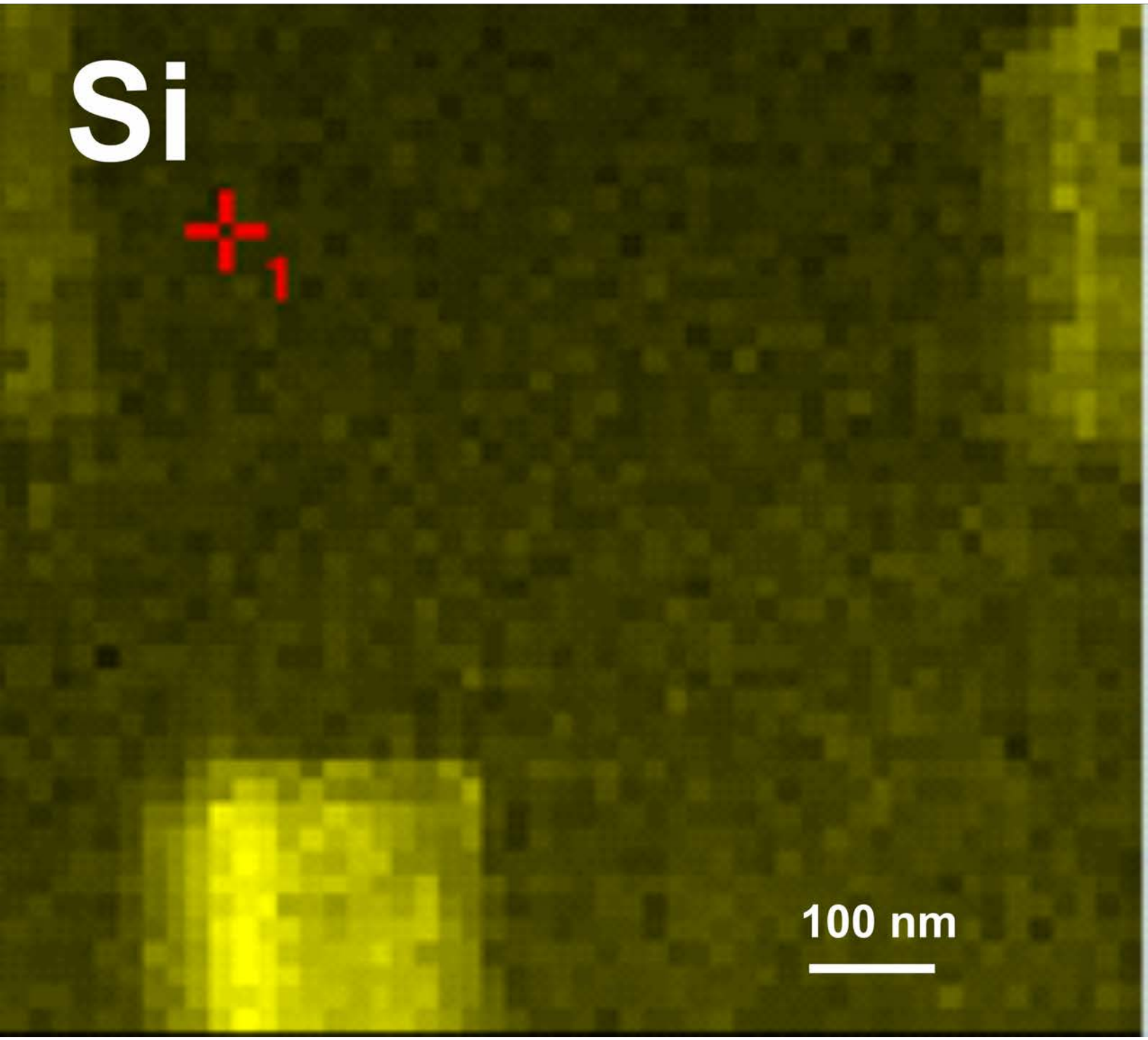

Figure 5b

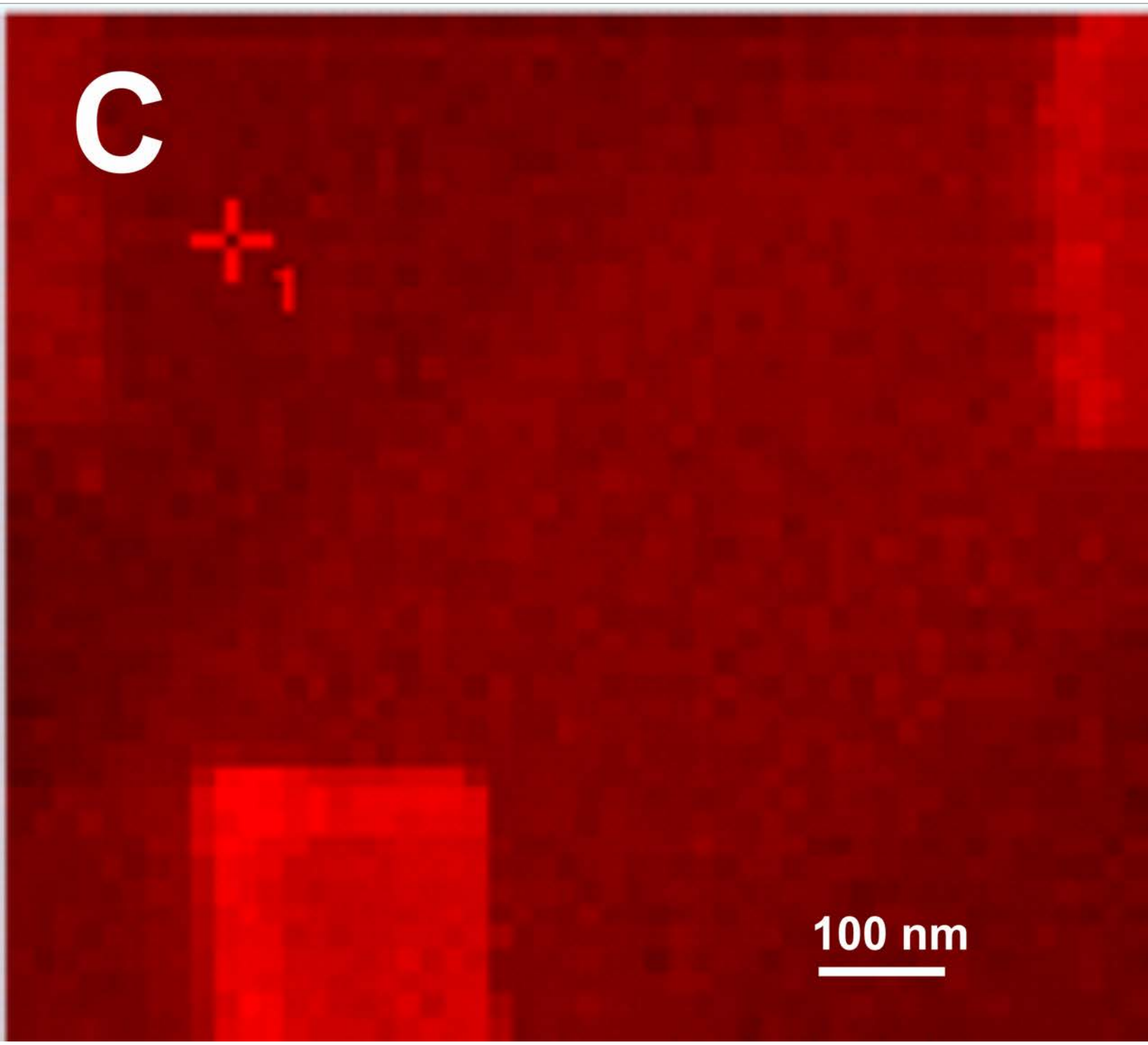

Figure 6

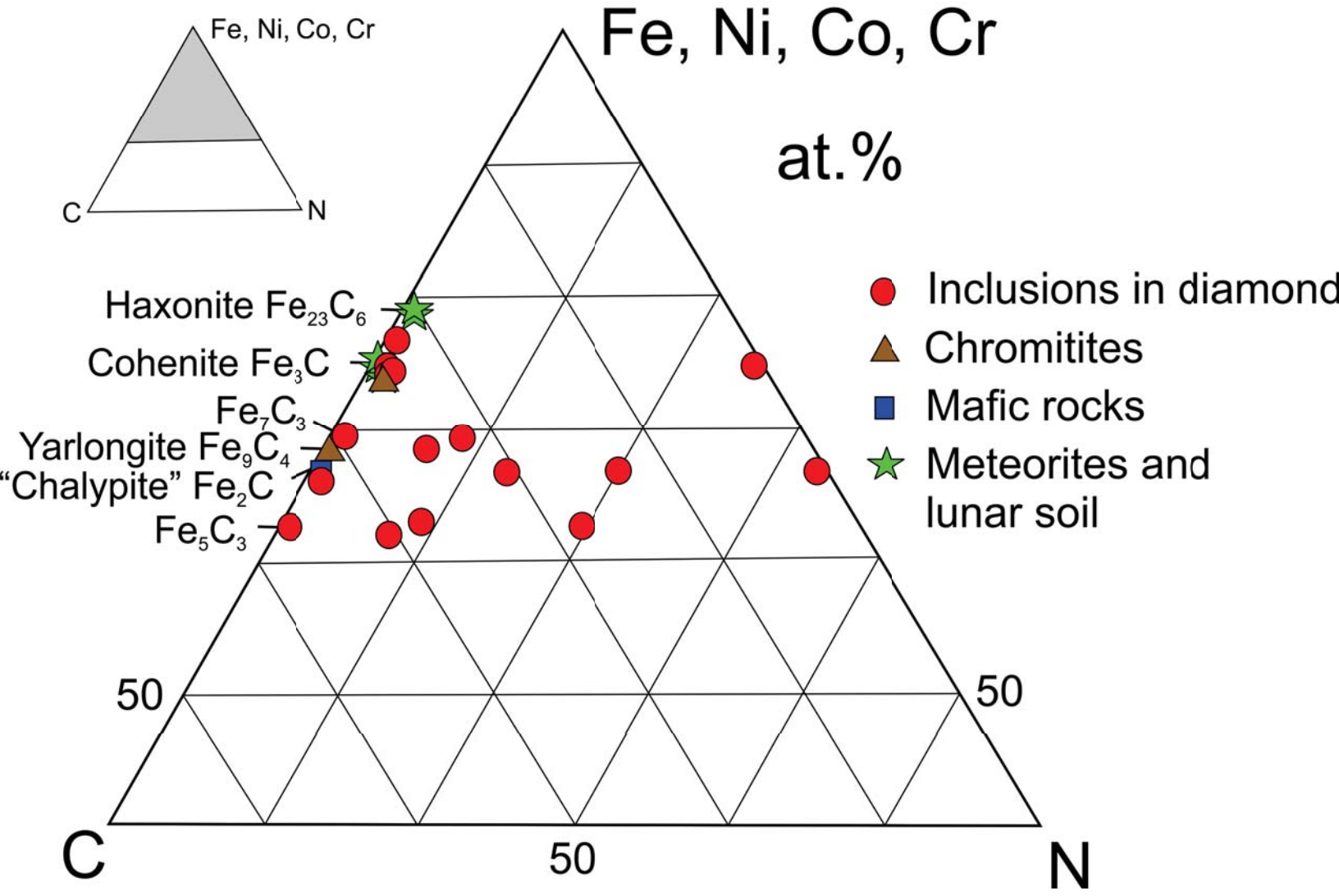
Fe, Ni, Co, Cr
C
N
Fe, Ni, Co, Cr
at.%
Haxonite $Fe_{23}C_6$
Cohenite Fe_3C
Fe_7C_3
Yarlongite Fe_9C_4
"Chalypite" Fe_2C
Fe_5C_3
Inclusions in diamond
Chromitites
Mafic rocks
Meteorites and lunar soil
50
50
50
C
N

Table 1. List of samples

Foil #	Major inclusions	Mineral phases
2327	Three grains of iron nitride	Fe_3N trigonal or Fe_2N orthorhombic
2934	Single nitride-graphite grain	Fe_2N orthorhombic
4592	Nitride + graphite Oxides	Fe_3N trigonal (b) (Fe-Mn) cubic (c) (Mn-Fe-Cr) orthorhombic (d) (Cr-Mn-Fe) orthorhombic
4588	Multiphase: carbonitride + carbide + spinel	$Fe_9(N_{0.8}C_{0.2})_4$ trigonal (host) Fe_7C_3 orthorhombic (two lamellae) SiC within lamellae Cr-Mn-Fe spinel (cubic)

Table 2. Cation compositions of oxide grains, intergrown with nitride and carbonitride (in at.%)

Element	Foil #4588	Foil #4592		
	Cubic	Oxide “b” Cubic	Oxide “c” Orthorhombic	Oxide “d” Orthorhombic
Cr	60.80	-	23.07	56.17
Mn	29.01	61.00	46.05	25.29
Fe	7.57	37.56	28.09	13.31
V	1.27	-	1.31	3.38
Si	1.35	1.44	1.48	1.85
Total	100.00	100.00	100.00	100.00

Table 3. Summary on natural iron carbides and nitrides

Theoretic stoichiometries	At. ratio M/(C,N)	Natural compounds		
		Carbides (N/(C+N) < 0.1)	Nitrocarbides (N/(C+N) = 0.1-0.5) and carbonitrides (N/(C+N) = 0.5-0.9)	Nitrides (N/(C+N) > 0.9)
$M_5(C,N)_3$	1.67	Fe_5C_3 (Fe/C = 1.65-1.77) Incl. ##9, 10 in diamond [9]	Fe/(C+N) = 1.65-1.69 N = 0.19-0.24 Incl. ##12, 13 in diamond [9]	
$M_2(C,N)$	2.0	Fe_2C – "chalypite" (1) Niakornak iron [1]; (2) Incl. ##1, 2, 5, 7 in diamond (Fe/C = 1.95-2.14) [9]	Fe/(C+N) = 1.5-2 N/(C+N) = 0.37-0.60 Incl. in diamond [10]	Fe_2N orthorhombic [11]
$M_9(C,N)_4$	2.25	$(Fe,Cr,Ni)_9C_4$ – yarlongite Chromitite [8]	$Fe_9(N_{0.8}C_{0.2})_4$ trigonal N/(C+N) = 0.2 [11]	
$M_7(C,N)_3$	2.33	Fe_7C_3 orthorhombic [11]	Fe/(C+N) = 2.32 N/(C+N) = 0.27 Incl. #14 in diamond [9]	
$M_5(C,N)_2$	2.5		$Fe_5(C,N)_2$ (Fe/(C+N) = 2.52) N/(C+N) = 0.54 Incl. in diamond [10]	
$M_3(C,N)$	3.0	$(Fe,Ni,Co)_3C$ – cohenite (1) Iron meteorites [3]; (2) Lunar soil [4, 5]; (3) Incl. in diamond [3, 7, 9]; (4) Chromitites [8]; (5) Basaltic rocks		Fe_3N trigonal [11]
$M_{10}(C,N)_3$	3.33	$Fe_{10}C_3$ (Fe/C = 3.33-3.59) Incl. ##3, 8, 11 in diamond [9]		
$M_{23}(C,N)_6$	3.83	$(Fe,Ni,Co)_{23}C_6$ – haxonite (1) Iron meteorites [2, 3]; (2) Incl. #6 in diamond (Fe/C = 3.98) [9]		

References: [1] - Shepard, 1867; [2] - Scott 1971; [3] Buchwald 1975; [4] - Goldstein et al. 1976; [5] Barsukov and Tarasov 1982; [6] – Bulanova and Zayakina 1991; [7] – Jacob et al. 2004; [8] - Shi et al 2009; [9] - Kaminsky & Wirth 2011; [10] - Kaminsky et al. 2015; [11] – this work.